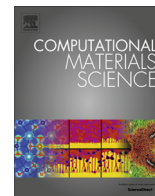




Contents lists available at ScienceDirect

Computational Materials Science

journal homepage: www.elsevier.com/locate/commatsci

Mechanical properties and electronic structures of diverse Pt–Al intermetallics: First-principles calculations



Yan Zhao^a, Jinku Yu^{a,*}, Lailei Wu^{a,*}, Biao Wan^{a,b}, Yunkun Zhang^a, Rui Gao^c, Jingwu Zhang^a, Huiyang Gou^b

^a Key Laboratory of Metastable Materials Science and Technology, College of Material Science and Engineering, Yanshan University, Qinhuangdao 066004, China

^b Center for High Pressure Science and Technology Advanced Research, Shanghai 201203, China

^c Key Laboratory of Applied Chemistry, College of Environmental and Chemical Engineering, Yanshan University, Qinhuangdao 066004, China

ARTICLE INFO

Article history:

Received 12 April 2016

Received in revised form 1 August 2016

Accepted 3 August 2016

Keywords:

Pt–Al intermetallics

Phase stability

Mechanical property

Electronic structure

First-principles calculations

ABSTRACT

Binary Pt–Al intermetallics are of growing interest in high-temperature technology. Here we investigate the structural stability, mechanical property and electronic structure of Pt–Al intermetallics by means of first-principles techniques. Our results reproduce the stable phases, Pt₅Al₃, α-PtAl, α-Pt₂Al₃, and PtAl₂. *I4/mcm*-PtAl₅ is firstly predicted to be stable phase. The bulk moduli of Pt–Al intermetallics generally enhance with the increasing of Pt concentration. The *Pmm*-Pt₃Al exhibits the maximum values of bulk, shear and Young's modulus among all Pt–Al intermetallics, while PtAl₅ also possesses outstanding shear and Young's modulus among Al-rich phases. Al-3*p* electrons are delocalized for all Pt–Al intermetallics, while the delocalization of Pt-5*d* electrons only shows up in Pt-rich phases. Relatively strong hybridization between Al–Al atoms for PtAl₅, and Pt–Al atoms for *Pm* $\bar{3}$ *m*-Pt₃Al, is crucial to understand their outstanding structural stabilities and mechanical properties.

© 2016 Elsevier B.V. All rights reserved.

1. Introduction

Intermetallics formed by aluminum and transition metals or noble metals are of high interesting for high-temperature applications, due to the good oxygen resistance, low density and price, in comparison with the pure transition metal or noble metal [1–7]. Especially, binary Pt–Al intermetallics achieve growing interests for high temperature coating materials, e.g. for gas turbine blades or car engines, due to remarkable high-temperature strength, high melting points and good oxidation resistance. In the past decades, diverse phases, such as PtAl, Pt₃Al, Pt₅Al₃, Pt₂Al₃, PtAl₂, Pt₈Al₂₁, PtAl₄, PtAl₅, and PtAl₆ have been reported in Pt–Al system [8–16]. Pt₃Al exhibits a cubic structure at high temperature (HT-Pt₃Al, *Pm* $\bar{3}$ *m* symmetry) and transforms to a tetragonal distortion (*P4/mbm* symmetry) upon cooling. The low temperature phase, denoted as LT-Pt₃Al, is closely related to the structure of Pt₃Ga [8–11]. Pt₂Al has a PbCl₂-type orthorhombic structure (HT-Pt₂Al) above 1060 °C, and below it shows a Pt₂Ga-type orthorhombic structure (LT-Pt₂Al) [12]. PtAl possesses a cubic FeSi-type structure (α-PtAl) at equilibrium condition, while a high-temperature β phase with NiAl-type structure is stable over

1260 °C [13]. Also, a rhombohedral PdAl-type PtAl (γ-PtAl film) was prepared by self-propagating, high temperature combustion synthesis [13]. As γ-PtAl was heated in air, an intermediate phase Pt₅Al₃ formed between 400 and 700 °C. At higher temperature, the alloy decomposed to be Pt and Al₂O₃ in air [14]. For Al-rich phases, PtAl₂ adopts the fluorite-type structure, and the duplex-phase layer (PtAl₂ + NiAl) exhibited excellent oxidation resistance at 1100 °C [15]. With higher Al concentration, Pt₃Al₁₁, PtAl₄, PtAl₅ and PtAl₆ have been observed in experiment for a long time, however, to the best of our knowledge, their crystal structures are not fully understood till now, due to the difficulty of structural determinations [16–20]. Hitherto, extensive researches have been focused on the understanding of synthesis conditions and thermodynamic stability (e.g. formation enthalpy) of Pt–Al phases. Unfortunately, the reports on the mechanical properties are limited both experimentally and theoretically [21,22], although, the knowledge of mechanical properties also plays a vital role for technological applications for Pt–Al phases. Moreover, a general understanding of structure types, mechanical properties and the relationship with electronic property is not performed for Pt–Al system, which may facilitate the understanding of possible synthesis condition, stabilities and applications. Nowadays, the advancements of *ab initio* calculations allow the theoretical modeling of new materials, which can predict their physical properties and give the suggestion

* Corresponding authors.

E-mail addresses: yujinku@ysu.edu.cn (J. Yu), wll@ysu.edu.cn (L. Wu).

of new syntheses route. Therefore, by using first principles calculations, a systematical investigation on stability, crystal structure, mechanical property and electronic structure were performed here, the obtained results will be extremely useful for understanding and developing Pt–Al intermetallics.

2. Calculation details

The calculations were performed by using Cambridge Serial Total Energy Package (CASTEP) code based on density functional theory (DFT) [23]. Ultrasoft pseudopotentials (USPPs) were used for electron-ion interactions [24], and plane waves were employed for the electronic wave function expansion. The generalized gradient approximation with Perdew-Burke-Ernzerhof (GGA-PBE) was employed to evaluate exchange-correlation energy [25]. The valence electron configurations were treated as Pt: $5d^96s^1$ and Al: $3s^23p^1$. A cutoff energy of 400 eV and a dense k -points in Brillouin zone by Monkhorst-Pack scheme [26] were selected to ensure a good convergence of total energy within 1 meV per formula units. The spin polarized was included for Pt-rich phases, and the magnetism was found to be neglected. Hooke's law was employed to calculate the elastic constants (C_{ij}). Bulk moduli (B) and shear moduli (G) were calculated within Voight-Reuss-Hill (VRH) approximation [27,28]. Young's modulus (E) and Poisson's ratio (ν) were obtained with the equations: $E = 9BG/(3B + G)$, $\nu = (3B - 2G)/(6B + 2G)$. Because the chemical related compounds usually share a similar structure, we carry out a massive structural search for Al-rich phases with stoichiometry close to 1:4, 1:5 and 1:6 based on the International Crystallographic Structure Database (ICSD), more than thirty combinations of {Ni, Pd, Ru, La, Au}–{Al, Ga, In} crystal structures were considered. After a full stress and position relaxation, structures related to La_3Al_{11} , $PdGa_5$ and $PtGa_6$ were obtained with relatively lower formation enthalpy for Pt_3Al_{11} , $PtAl_5$ and $PtAl_6$, respectively.

3. Results and discussion

3.1. Lattice structure and thermodynamic stability

All of the Pt–Al intermetallics considered here are visualized by polyhedrons (as shown in Fig. 1). In Pt-rich phases (Fig. 1a–e), two types Pt atoms, Pt_c (locating at center) and Pt_v (locating at vertex) can be found in the polyhedron. Each Pt_c atom is coordinated by twelve atoms, forming $Pt_c@M_{12}$ polyhedrons ($M = Pt_v$ or Al). The $Pt_c@M_{12}$ cuboctahedron in HT-Pt₃Al (Fig. 1a) can be viewed as an eight corner-truncated cube, each Pt_c atom is coordinated by eight Pt_v atoms and four Al atoms. In LT-Pt₃Al, $Pt_c@M_{12}$ is slightly distorted to adapt a lower symmetry (Fig. 1b). Significant distorted $Pt_c@Pt_v_5Al_7$ and $Pt_c@Pt_v_6Al_6$ polyhedrons can be found in HT-Pt₂Al and Pt₅Al₃ (Fig. 1c and e). In LT-Pt₂Al (Fig. 1d), two types distorted quadrangular prisms, $Pt_c@Pt_v_8Al_4$ and $Pt_c@Pt_v_6Al_6$, are formed. In Al-rich side (including PtAl phases), Pt atoms are all coordinated by Al atoms, and diverse $Pt_c@Al_x$ ($x = 7, 8, 9$ and 10) polyhedrons can be observed. $Pt_c@Al_7$ polyhedron and $Pt_c@Al_8$ cube are the structural unit of α -PtAl (Fig. 1f) and β -PtAl (Fig. 1g), respectively; and both of them are shown up in γ -PtAl (Fig. 1i). $Pt_c@Al_8$ cube can also be found in PtAl₂ (Fig. 1j) and α -Pt₂Al₃ (slightly distorted as shown Fig. 1j). For β -Pt₂Al₃, Pt₈Al₂₁, Pt₃Al₁₁ and PtAl₄, the complex structures are formed by more than two types of $Pt_c@Al_x$ polyhedrons (Fig. 1k, m–o). Very intriguingly, PtAl₅ possesses a high symmetrical structure with close packed $Pt_c@Al_{10}$ small icosahedrons, different from other Al-rich phases. It should be pointed out that, $Pt_c@Al_x$ with the same x value in different phases (sometime in the same phase) only represent the same coordination number. For example, in $P\bar{1}$ -PtAl₆, the bond

lengths in $Pt_c@Al_9$ polyhedrons are quite different from each other because of the low symmetry.

The calculated lattice parameters and formation enthalpy are shown in Table 1. Our calculated lattice parameters are in good agreement with the experimental and theoretical results with an error of less than 2.0%, suggesting the good reliability. Thermodynamic stability of Pt_xAl_y was examined firstly by constructing a convex-hull of the formation enthalpy with respect to *fcc*-Al and *fcc*-Pt. The formation enthalpy, ΔH_f , of Pt_xAl_y after full structural relaxation was evaluated as following:

$$\Delta H_f = E_{Pt_xAl_y} - (xE_{Pt} + yE_{Al}) \quad (1)$$

Here, $x + y = 1$, $E_{Pt_xAl_y}$, E_{Al} and E_{Pt} , are total energy of Pt_xAl_y , *fcc*-Al and *fcc*-Pt, respectively. The calculated ΔH_f also agrees well with previous reports [23,29], further indicating the good reliability. As shown in Fig. 2a, the experimental phases, Pt₅Al₃, α -PtAl, α -Pt₂Al₃, PtAl₂, are just staying on the convex-hull (solid line), suggesting the thermodynamic stability, consistent with previous theoretical and experimental results [22,29]. HT-Pt₃Al, LT-Pt₂Al, and Pt₈Al₂₁ are slightly above the convex-hull, indicating their metastable nature. ΔH_f of β -PtAl and β -Pt₂Al₃ are highly above the convex-hull, their stability at elevated temperature should contribute to the entropy effect. ΔH_f of α -PtAl ($-113.15 \text{ kJ}\cdot\text{mol}^{-1}\cdot\text{atom}^{-1}$) and γ -PtAl ($-109.11 \text{ kJ}\cdot\text{mol}^{-1}\cdot\text{atom}^{-1}$) are very close, reasonable interpreting their experimental observations at room conditions [29]. Abnormally, a slight ΔH_f difference was found between the high-temperature phase HT-Pt₂Al ($-93.72 \text{ kJ}\cdot\text{mol}^{-1}\cdot\text{atom}^{-1}$) and the low-temperature phase LT-Pt₂Al ($-93.43 \text{ kJ}\cdot\text{mol}^{-1}\cdot\text{atom}^{-1}$) at zero temperature and zero pressure. The ΔH_f of Al-rich phases, PtAl₆, PtAl₅, PtAl₄ and Pt₃Al₁₁ are firstly evaluated here. Interestingly, as shown in Fig. 2a, PdGa₅-type PtAl₅ stays on the convex-hull. Furthermore; there is no imaginary frequency found in the whole Brillouin zone (as shown in Fig. 2b). Therefore, PdGa₅-type PtAl₅ is both thermodynamically and dynamically stable at 0 K and 0 GPa. PtAl₅ has also been reported experimentally over four decades [20], but there was not any structural information reported. Our prediction may be a good candidate for future experimental identification. $P\bar{1}$ -PtAl₆, $P3c1$ -PtAl₄ and $P1$ -Pt₃Al₁₁ are metastable with about 1.78, 3.38, and $4.55 \text{ kJ}\cdot\text{mol}^{-1}\cdot\text{atom}^{-1}$ above convex hull, respectively.

3.2. Mechanical property

Pt–Al intermetallics are usually utilized as thermal barrier coatings of turbine blades of jet engines and gas turbines. Mechanical properties play a vital role for their technological applications. The measurement of individual elastic constants (C_{ij} s) of the thin films is difficult. By a strain-stress method, C_{ij} s can be calculated at zero pressure and zero temperature. A small finite strain was applied on the optimized structure and then the elastic constants were obtained from the stress of the strained structure. Mechanical stability was examined firstly with the Born-Huang mechanical stability criteria [28,30], which can be expressed as:

For cubic structure, $C_{11} > 0$, $C_{44} > 0$, $C_{11} - C_{12} > 0$ and $C_{11} + 2C_{12} > 0$;

For hexagonal structure, $C_{44} > 0$, $C_{11} - |C_{12}| > 0$ and $(C_{11} + 2C_{12})C_{33} > 2C_{13}^2$;

For trigonal structure, $C_{11} > |C_{12}|$, $(C_{11} + C_{12})C_{33} - 2C_{13}^2 > 0$, $(C_{11} - C_{12})C_{44} - 2C_{14}^2 > 0$;

For orthorhombic system: $C_{11} > 0$, $C_{22} > 0$, $C_{33} > 0$, $C_{44} > 0$, $C_{55} > 0$, $C_{66} > 0$, $C_{11} + C_{22} + C_{33} + 2C_{12} + 2C_{13} + 2C_{23} > 0$, $(C_{11} + C_{22} - 2C_{12}) > 0$, $(C_{11} + C_{33} - 2C_{13}) > 0$, $(C_{22} + C_{33} - 2C_{23}) > 0$.

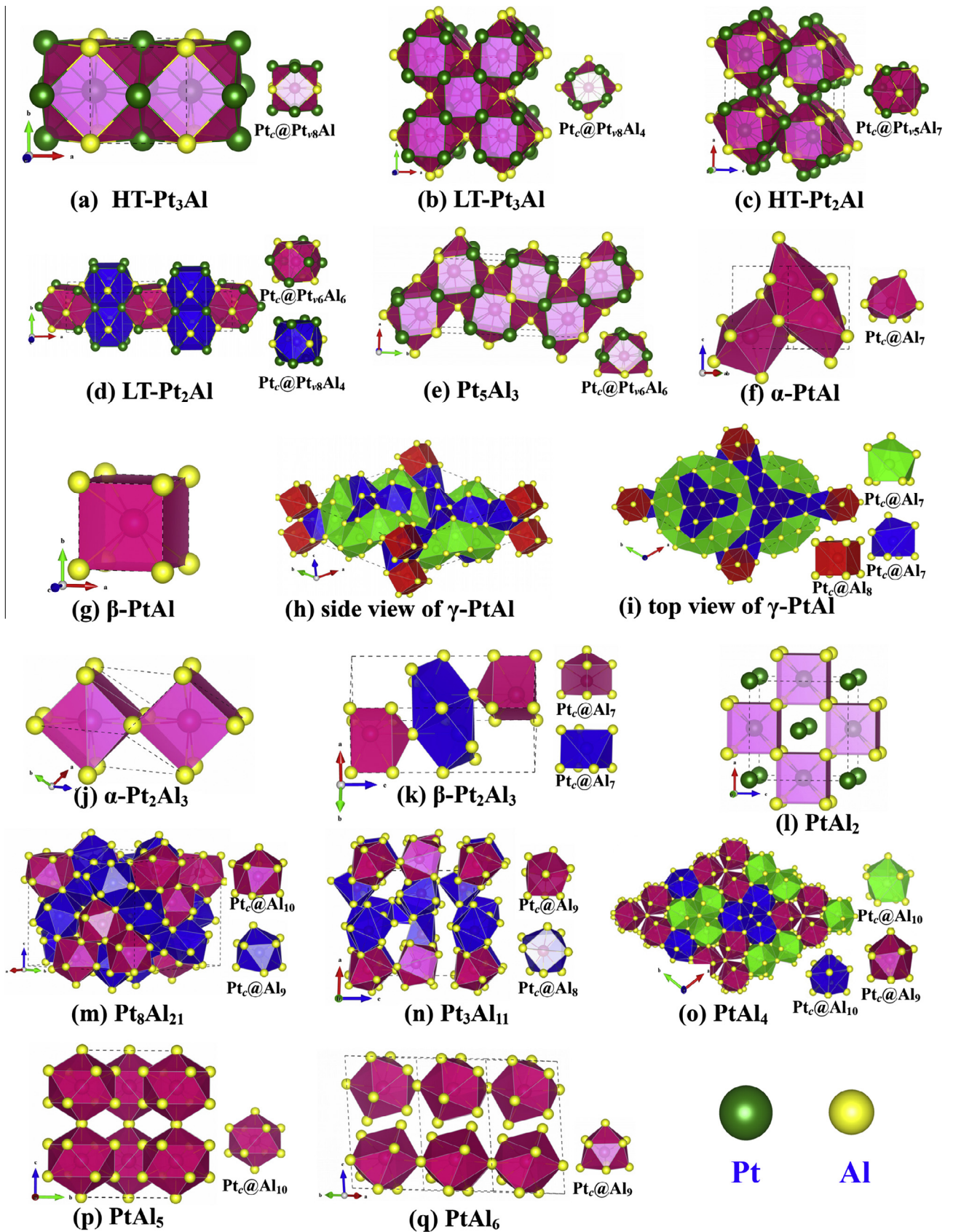


Fig. 1. Crystal structures Pt_xAl_y in view of polyhedron. Pt_c and Pt_v represent the center Pt atom and the vertex Pt atom in the polyhedron, respectively. It should be pointed out that, $Pt_c@Al_x$ with the same x value in different phases (sometime in the same phase) only represent the same coordination number.

Table 1Crystal parameters (*a*, *b*, and *c* in Å) and formation enthalpy (ΔH_f in $\text{kJ}\cdot\text{mol}^{-1}\cdot\text{atom}^{-1}$) for Pt_xAl_y in comparison with available theoretical and experiment results.

Phase	S.G.	Prototype	This work				Previous calculation			Experiment			
			<i>a</i>	<i>b</i>	<i>c</i>	ΔH_f	<i>a</i>	<i>b</i>	<i>c</i>	<i>a</i>	<i>b</i>	<i>c</i>	ΔH_f
Pt	<i>Fm</i> $\bar{3}m$		4.00				3.924 ^b			3.887 ^a			
LT-Pt ₃ Al	<i>P4</i> / <i>mbm</i>	Pt ₃ Ga	5.53		7.96	-76.77	5.463 ^b		7.829	5.46 ^d	7.820		-71.1 ^c
HT-Pt ₃ Al	<i>Pm</i> $\bar{3}m$	Cu ₃ Au	3.94			-74.17	3.895 ^b			3.876 ^e			-69.9 ^f
LT-Pt ₂ Al	<i>Pmma</i>	Pt ₂ Ga	16.49	3.97	5.52	-93.43	16.39 ^b	3.908	5.459	16.30 ^f	3.921	5.439	-88.0 ^f
HT-Pt ₂ Al	<i>Pnma</i>	PbCl ₂	5.49	4.12	7.96	-93.72	5.421 ^b	4.073	7.864	5.401 ^f	4.055	7.898	-87.3 ^f
Pt ₅ Al ₃	<i>Pbam</i>	Rh ₅ Ge ₃	5.48	10.84	4.03	-99.86	5.406 ^b	1072	3.975	5.41 ^e	10.70	3.95	-87.8 ^f
α -PtAl	<i>P2</i> 13	FeSi	4.92			-113.15	4.868 ^b			4.864 ^c			-101 ^f
β -PtAl	<i>Pm</i> $\bar{3}m$	CsCl	3.09			-105.21	3.043 ^b			3.125 ^c			-100 ^f
γ -PtAl	<i>R</i> $\bar{3}$		15.78		5.36	-109.11				15.571 ^g		5.304	
α -Pt ₂ Al ₃	<i>P</i> $\bar{3}m$ 1	Ni ₂ Al ₃	4.24		5.22	-108.76	4.185 ^b		5.140	4.208 ⁱ		5.172	-94.9 ^f
β -Pt ₂ Al ₃	<i>P</i> $\bar{3}m$ 1		4.16		10.90	-73.36							
PtAl ₂	<i>Fm</i> $\bar{3}m$	CaF ₂	5.94			-99.08	5.84 ^b			5.910 ^e			-90.0 ^f
Pt ₈ Al ₂₁	<i>I4</i> 1/ <i>a</i>	Pt ₈ Al ₂₁	13.05		10.76	-81.44				12.96 ^j		10.68	-71.3 ^f
Pt ₃ Al ₁₁	<i>P</i> 1	La ₃ Al ₁₁	10.42	8.79	10.20	-61.47							
PtAl ₄	<i>P</i> 3 <i>c</i> 1		13.21		9.68	-58.59				13.077 ^k		9.634	
PtAl ₅	<i>I4</i> / <i>mcm</i>	PdGa ₅	6.41		10.02	-53.00							
PtAl ₆	<i>P</i> $\bar{1}$	PtGa ₆	15.09	13.18	9.48	-43.58							
Al	<i>Fm</i> $\bar{3}m$		4.05				4.05 ^b			4.05 ^a			

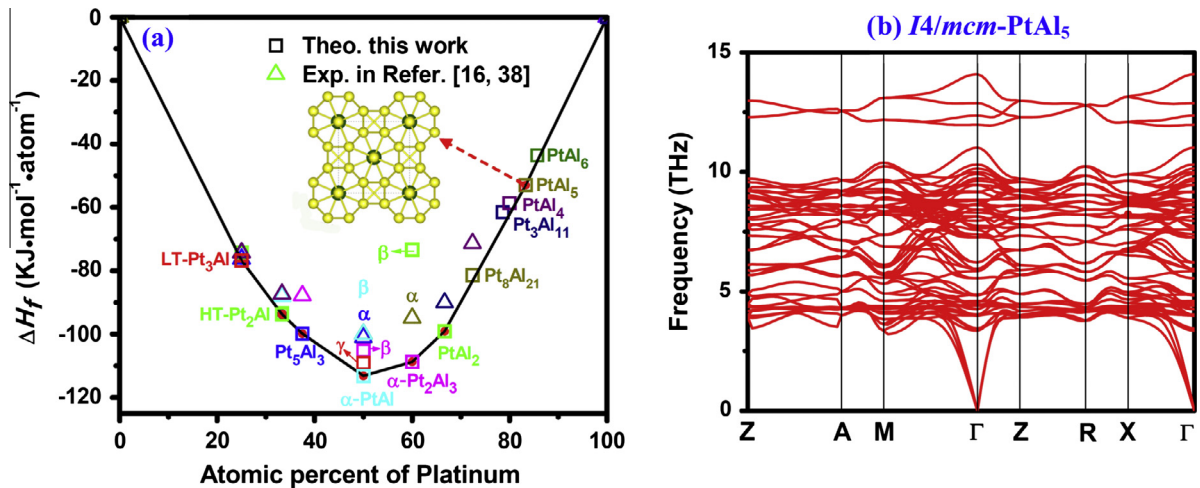
^a Exp. in Ref. [35];^b Cal. in Ref. [22];^c Exp. in Ref. [36];^d Exp. in Ref. [37];^e Exp. in Ref. [29];^f Exp. in Ref. [16];^g Exp. in Ref. [13];^h Exp. in Ref. [14];ⁱ Exp. in Ref. [38];^j Exp. in Ref. [39];^k Exp. in Ref. [17].

Fig. 2. Calculated formation enthalpy of Pt–Al intermetallics (a), the square represent calculated results of this work and triangles represent experimental values in reference (9, 35), the red solid circles represent stable phases; calculated phonon dispersion curves of PtAl₅ (b). (For interpretation of the references to colour in this figure legend, the reader is referred to the web version of this article.)

More detailed expression can be referred in [28,31]. As shown in Table 2, all of the Pt_xAl_y phases satisfy the Born-Huang mechanical stability criteria, demonstrating they are mechanical stable. A general rule is that C_{11} , C_{22} , and C_{33} are greater than C_{44} , and they are gradually increased with Pt concentration. Intriguingly, C_{33} of PtAl₅, 266 GPa, is the biggest one among the C_{11} , C_{22} and C_{33} of the Al-rich phases. While among the Pt-rich phase, LT-Pt₃Al phase has the largest C_{11} (354 GPa), which is also far greater than that of Ni₃Al (230 GPa) [1] and Ti₃Al (175 GPa) [32]. The large C_{33} of PtAl₅ and C_{11} of LT-Pt₃Al indicate their remarkably high strength along

[001] and [100] direction and good capability for coating applications.

To further demonstrate the mechanical properties of Pt_xAl_y , the elastic moduli calculated by Voight-Reuss-Hill (VRH) [27] method are listed in Table 2 and Fig. 3. Generally, the bulk modulus decreases with Pt concentration (as shown in Fig. 3), from 257 GPa for *fcc*-Pt to 74 GPa for *fcc*-Al, which should ascribe to the higher valence density of Pt. Note that similar tendency has also been found for Ru–Al [4] and Ni–Al [2]. Shear modulus and Young's modulus share a similar trend, with the maximum value

Table 2
Elastic constants (C_{ij} in GPa), bulk modulus (B in GPa), shear modulus (G in GPa), Yong's modulus (E in GPa), and Poisson's ratio (ν) of Pt_xAl_y intermetallics.

	C_{11}	C_{22}	C_{33}	C_{44}	C_{55}	C_{66}	C_{12}	C_{13}	C_{23}	B	G	B/G	E	ν
Pt	332			78			219			257	68	3.779	188	0.38
	349.7			61			170.2			230	71.1	3.235	193	0.360 ^a
	355.8			62.3			191			246.9	71.23	3.466	192	0.368 ^b
LT-Pt ₃ Al	354		329	96		57	140	179		226	84	2.71	223	0.31
	398.8		386.2	111.9		63.9	162.8	214.0		262.5	94.3	2.784	273.2	0.335 ^b
HT-Pt ₃ Al	343			116			179			234	101	3.37	264	0.34
	331.6			72.4			193.2			239.3	71.08	3.367	194	0.365 ^b
LT-Pt ₂ Al	336	317	347	105	57	107	162	135	162	213	87	2.45	230	0.32
	309.1	317.5	366.5	108.6	69.5	110	171.6	143.8	170	217.2	89.1	2.438	236.1	0.320 ^b
HT-Pt ₂ Al	306	309	305	68	45	80	165	148	174	210	66	3.18	180	0.36
	310.8	315.8	314.4	63.6	51.2	76.7	173.3	158.2	178.8	217.8	66.25	3.288	180.4	0.362 ^b
Pt ₂ Al ₃	307	269	290	58	77	34	135	165	180	202	57	3.55	156	0.31
	284.1	285.1	286.6	58.1	87.8	67.79	157.4	204.6	185.6	216	60.93	3.545	167.1	0.371 ^b
α -PtAl	297			75			134			188	84	2.42	218	0.32
	361.2			103.2			128.7			206.2	108.2	1.906	276.4	0.277 ^b
β -PtAl	284			84			142			189	78	2.42	206	0.32
	315.4			80.0			136.6			198	82.9	2.388	230	0.316 ^b
γ -PtAl	291		289	62			138	126		184	71	2.59	189	0.33
α -Pt ₂ Al ₃	245		281	71			100	103		153	74	2.08	191	0.29
	351.8		291.8	80.6			144.7			190.8	93.9	2.032	242	0.289 ^b
β -Pt ₂ Al ₃	204		151	38			118	92		126	41	3.08	111	0.35
PtAl ₂	204			86			93			130	72	1.80	182	0.27
	237.9			74.5			107.9			151.2	61.02	2.478	183.2	0.322 ^b
Pt ₈ Al ₂₁	229		199	70		58	93	90		133	64	2.08	165	0.29
	246.7		215.5	73.2		62.96		103.5		142.1	69.84	2.035	180.3	0.289 ^b
Pt ₃ Al ₁₁	178	183	188	49	51	25	55	52	55	97	44	2.26	112	0.40
PtAl ₄	167		240	19			90	63		112	34	3.27	93	0.36
PtAl ₅	205		266	69		63	49	42		104	76	1.38	182	0.21
PtAl ₆	207	183	133	71	68	61	57	50	66	94	59	1.59	147	0.24
Al	144			41			41			74	35	2.12	91	0.30
	107			28			61			76	26	2.923	70	0.346 ^c
	106.8			29.31			56.95			73.6	27.5	2.676	73.3	0.334 ^b

^a Exp. in Ref. [40];
^b Cal. in Ref. [22];
^c Exp. in Ref. [41].

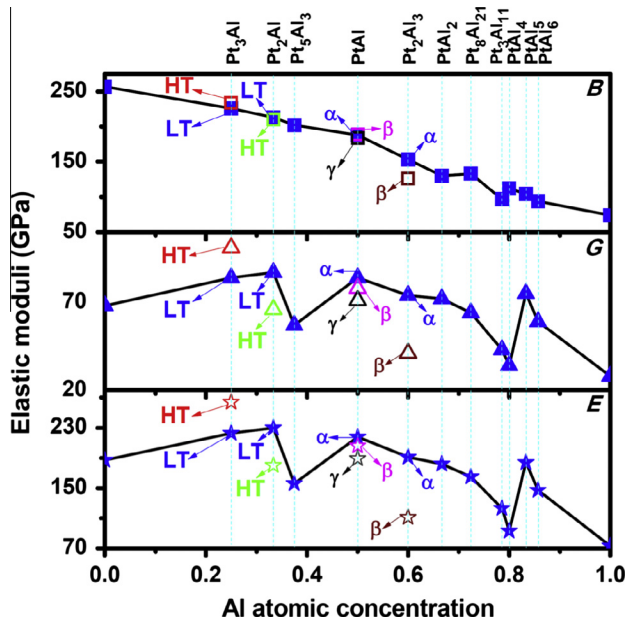


Fig. 3. The functions of bulk modulus (B), shear modulus (G) and Young's modulus (E) vs Al concentration for Pt_xAl_y intermetallics.

located at HT-Pt₃Al ($G = 101$ GPa, $E = 264$ GPa), and minimum value from PtAl₄ ($G = 34$ GPa, $E = 93$ GPa). The G and E of Pt₃Al are also greater than that of Ni₃Al ($G = 83$ GPa, $E = 217$ GPa) [3]. Additionally, G of LT-Pt₃Al, HT-Pt₃Al, LT-Pt₂Al, α -PtAl, β -PtAl, γ -PtAl, α -Pt₂Al₃, PtAl₂ and PtAl₅ are greater than pure metal Pt, while

others are between that of *fcc*-Pt and *fcc*-Al. For PtAl phases, B , G and E follow the sequence of $\beta > \alpha > \gamma$. Both G and E of α -PtAl ($G = 84$ GPa, $E = 218$ GPa) and β -PtAl ($G = 78$ GPa, $E = 206$ GPa), are about two times of NiAl ($G = 38.5$ GPa, $E = 107$ GPa) [2], and E of α - and β -PtAl are comparative with that of RuAl ($E = 232$ GPa) [4]. For Pt₂Al₃ and Pt₂Al, the low-temperature phases (α -Pt₂Al₃ and LT-Pt₂Al) possess greater B , G and E values in comparison with the corresponding high-temperature phases (β -Pt₂Al₃ and HT-Pt₂Al), which is just reverse for Pt₃Al phases. It should be noted that greater G (76 GPa) and E (182 GPa) values are also found for PtAl₅ among the Al-rich phases, just next to β -PtAl ($G = 78$ GPa) and α -Pt₂Al₃ ($E = 191$ GPa). This singularity may be derived from the Al–Al covalent bond, which will be analyzed in detail in the following section.

The brittle or ductile behaviors of materials can be evaluated by Pugh's ratio (B/G), with a critical value 1.75 [33]. B/G values of PtAl₆ and PtAl₅ are 1.59 and 1.38, less than 1.75, showing a brittle nature, while the others show the ductile feature. Poisson's ratio (ν) is usually used to describe the covalent bonding degree of a material. From Table 2, the Poisson's ratio of PtAl₅ is 0.21, much smaller than the others, indicating possible covalent bonding character.

Elastic anisotropy is an important parameter for coating materials. A three-dimensional (3D) surface and two dimensional (2D) projections of the Young's modulus as a function of the crystallographic direction were calculated and presented in the Supporting Information. The anisotropy of Young's modulus of the phases with prominent elastic moduli (i.e. HT-Pt₃Al, LT-Pt₃Al, LT-Pt₂Al, α -PtAl, β -PtAl and PtAl₅ with greater B , G , E as shown in Table 2 and Fig. 3) are shown in Fig. 4. A spherical shape in the three-dimensional (3D) surface and a circle in the corresponding 2D projection represent isotropic behavior [34], and the deviation

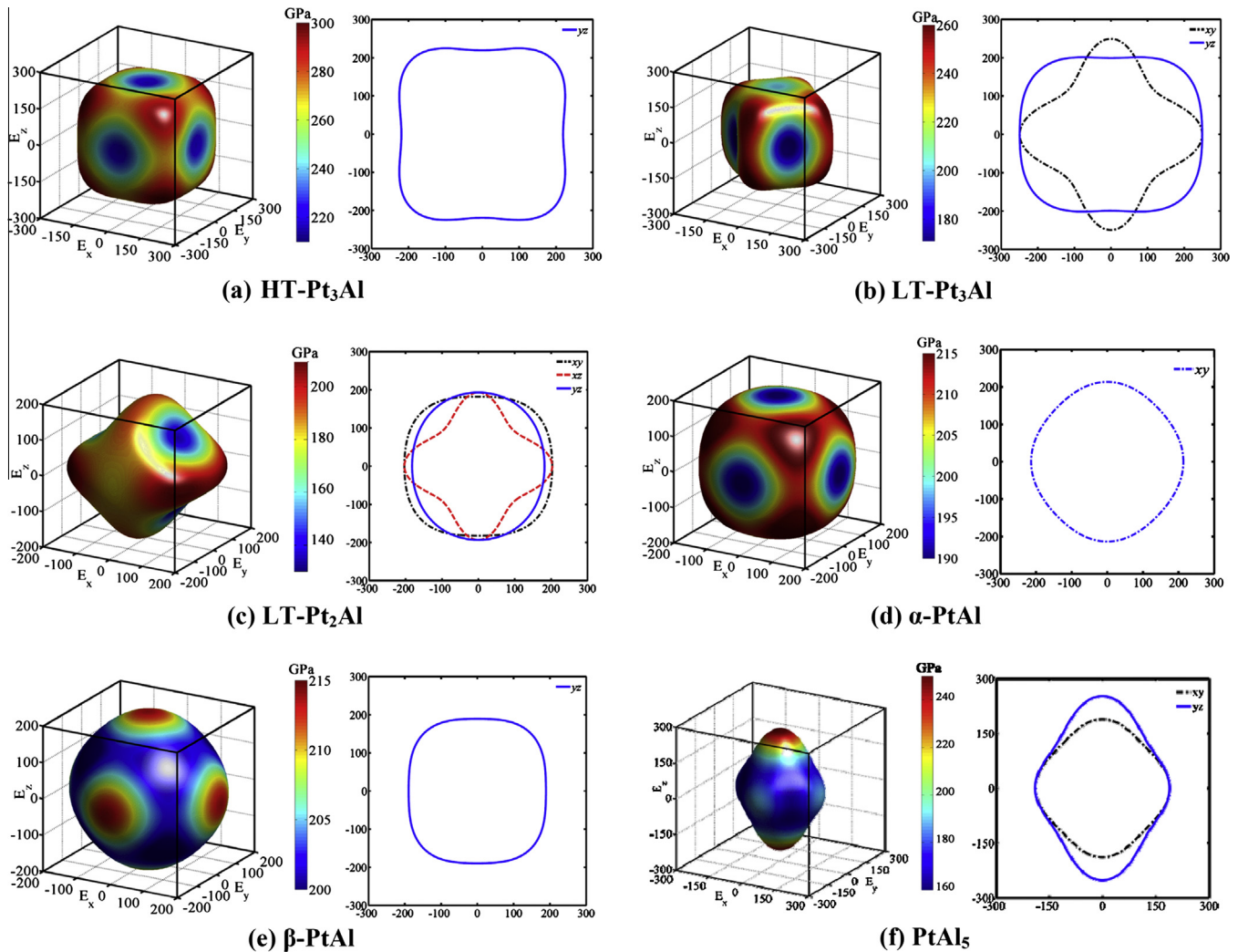


Fig. 4. Directional dependence and plane projections of Young's moduli. Note that the negative sign only denotes the direction corresponding to the positive one.

from the spherical shape/circle indicates the degree of anisotropy. As shown in Fig. 4d and e, from the 2D profile, very similar and nearly isotropic behavior can be observed for α -PtAl and β -PtAl, although they have different symmetry and coordination environments. However, from the 3D surface, the directions of maximum and minimum Young's modulus are reverse: $E_{\max} = 213.7$ GPa along [001], $E_{\min} = 198.6$ GPa along [111] for α -PtAl, $E_{\max} = 219.5$ GPa along [111] and $E_{\min} = 189.3$ GPa along [001] for β -PtAl. Slight anisotropy can be found for HT-Pt₃Al (Fig. 4a) with $E_{\max} = 298.6$ GPa along [111] and $E_{\min} = 220.2$ GPa along [001]. More anisotropy comes from PtAl₅, the highest and lowest Young's moduli are 252.1 GPa along [001] direction and 162.9 GPa along $[-0.640.65 - 0.42]$ direction with a difference of 90 GPa. Extreme anisotropy derives from LT-Pt₃Al and LT-Pt₂Al. For LT-Pt₃Al, $E_{\min} = 165.1$ GPa runs along $[-1 - 1 0]$, and $E_{\max} = 260.6$ GPa runs along $[0.850 - 0.53]$ directions, as for LT-Pt₂Al, $E_{\min} = 166.8$ GPa runs along $[10 - 1]$, and $E_{\max} = 271.2$ GPa runs along $[-0.79 - 0.620]$. We note that the E_{\max} of PtAl₅ (252.1 GPa) are comparative to that of LT-Pt₂Al (271.2 GPa) and higher than that of α -PtAl, β -PtAl, and LT-Pt₃Al, indicating its outstanding strength along [001] direction.

3.3. Electronic structure

To unveil the origin of the mechanical properties of Pt_xAl_y phases, total and partial density of states (TDOS and PDOS) are

calculated and plotted in Fig. 5. All of Pt_xAl_y phases exhibit metallic features due to the finite DOS values at Fermi level (E_F). For Pt-rich phases (Fig. 5a–e), the Fermi level was dominated by Pt-5d states with some contribution of Al-3p states. Pt-5d electrons are delocalized over a wide energy range ($-8, 3$) eV, indicating the Pt–Pt metallic bonding features. Also, the delocalization of Al-3p electrons can be found over all the valence band and conduction band, while Al-3s electrons are mostly localized at the lower energy part. Comparing with LT-Pt₃Al (Fig. 5a), relatively stronger hybridization between Al-3p and Pt-5d states can be observed for HT-Pt₃Al from -6 eV to -3 eV (Fig. 5b), indicating a stronger Pt–Al covalent bonding, which should be responsible for its greater G and E values. As going to α -PtAl (Fig. 5f), both s - p hybridization between Al atoms (-10 to -6.5) eV and strong p - d hybridization between Al and Pt atoms (-6.5 to 0) eV can be observed, which leads to a deep valley near Fermi level and well supports its special stability. With the increasing of Al content, the contributions of Al-3s and Al-3p states increase gradually while the reverse for Pt-5d state, and there is a narrow band gap at about -6.5 eV for PtAl₂ (Fig. 5k). In Al-rich phases with higher Al concentration, Pt₈Al₂₁, Pt₃Al₁₁, PtAl₄, PtAl₅, and PtAl₆ (Fig. 5l–p), DOS at Fermi level originated mostly from Al-3p states, and the contribution of Pt-5d states can be neglected. Both Al-3s and Al-3p electrons are delocalized from valence band to conduction band, while Pt-5d electrons become more localized, indicating the metallic feature of Al–Al bond. Furthermore, s - p hybridization between Al atoms is observed from

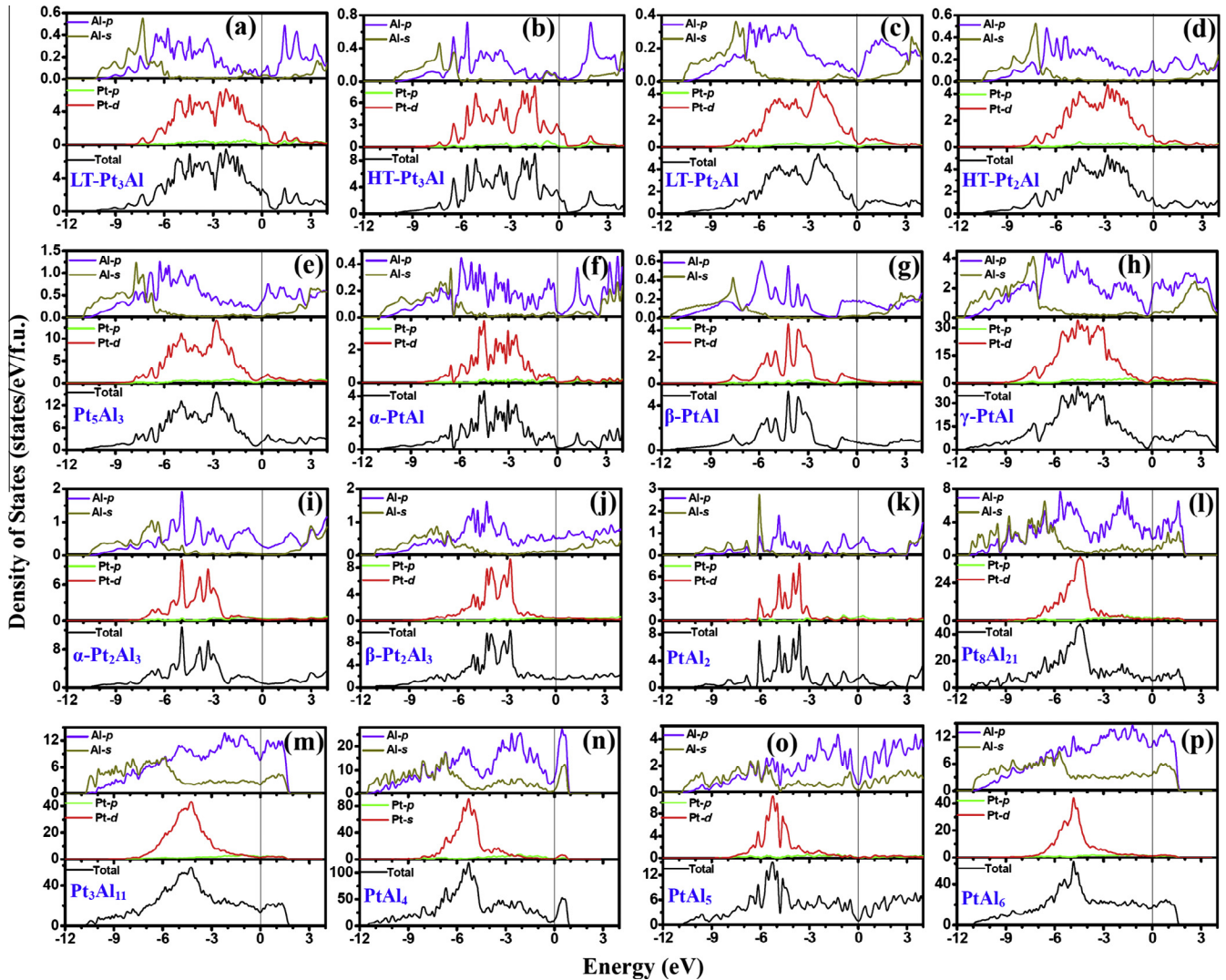


Fig. 5. Calculated total and partial density of states (TDOS and PDOS) of Pt–Al phases.

–10 to 5 eV, indicating the covalent Al–Al interactions. Particularly, for PtAl_5 , Al–Al covalent interactions are stronger than the other Al-rich phases with a very similar profile of Al-3s and Al-3p partial states over the valence band. And also, there are relatively high splitting for Al-3p and Pt-5d states between (–7, –3) eV, indicating the hybridization between Al-3p and Pt-5d orbitals. The strong hybridization in PtAl_5 results in a deep pseudogap at Fermi level, contributing the outstanding structural stability and mechanical property among the Al-rich phases.

To get a deeper insight of the bonding features, the valence charge density distributions of HT- Pt_3Al , α -PtAl and PtAl_5 have been calculated and displayed in Fig. 6. Near spherical shape of valence electrons on Pt and Al sites indicate the dominated metallic bonding characteristic. On the other hand, an electronic deviation from Al atom to Pt atom can be observed (in Fig. 6b–d), corresponding to a polar Pt–Al covalent interaction, due to the difference of electronegativity between Pt and Al atoms. For HT- Pt_3Al (Fig. 6a), electronic accumulations can also be found between Pt atoms, indicating Pt–Pt partial covalent character. Interestingly, electronic accumulations between Al–Al atoms are found along [010] direction for PtAl_5 (Fig. 6e), which should account for its great C_{33} value. The relatively strong covalent interactions in PtAl_5 are further confirmed by calculated Milliken overlap populations (MOP). The MOP values of Al–Al and Pt–Al bond in PtAl_5 are

0.64 and 0.54, bigger than that of Pt–Al bond (0.36) in α -PtAl, and Pt–Al (0.27) and Pt–Pt (0.12) bond in HT- Pt_3Al . Electronic transfer is also found in Pt–Al intermetallics, about 0.23–0.27 e for PtAl_5 , 0.48 e for α -PtAl, and 0.52 e for HT- Pt_3Al , are found transferring from Al to Pt atom, which is play an important role for good stabilities of PtAl_5 , α -PtAl and HT- Pt_3Al .

4. Conclusions

In summary, we have systematically explored the structural stability, mechanical properties and electronic structures of binary Pt–Al system. For Al-rich phases, $P\bar{1}$ -type PtAl_6 related to PtGa_6 , $P3c1$ - PtAl_4 and $P1$ -type $\text{Pt}_3\text{Al}_{11}$ related to $\text{La}_3\text{Al}_{11}$ are proposed to be metastable, and a hitherto unreported $I4/mcm$ - PtAl_5 is predicted to be stable in thermodynamics, dynamics and mechanics, which along with PtAl_2 , α - Pt_2Al_3 , α -PtAl, Pt_5Al_3 , HT- Pt_2Al and LT- Pt_3Al , construct the formation enthalpy convex-hull of Pt–Al system. Bulk modulus of Pt_xAl_y intermetallics generally decrease with Al concentration. Among Pt-rich phases, HT- Pt_3Al exhibits maximum values in B (234 GPa), G (101 GPa) and E (264 GPa); while for Al-rich phases, PtAl_5 possesses outstanding G (76 GPa) and E (182 GPa). By analyzing the electronic structures, a strong hybridization between Pt-5d and Al-3p orbitals is found in

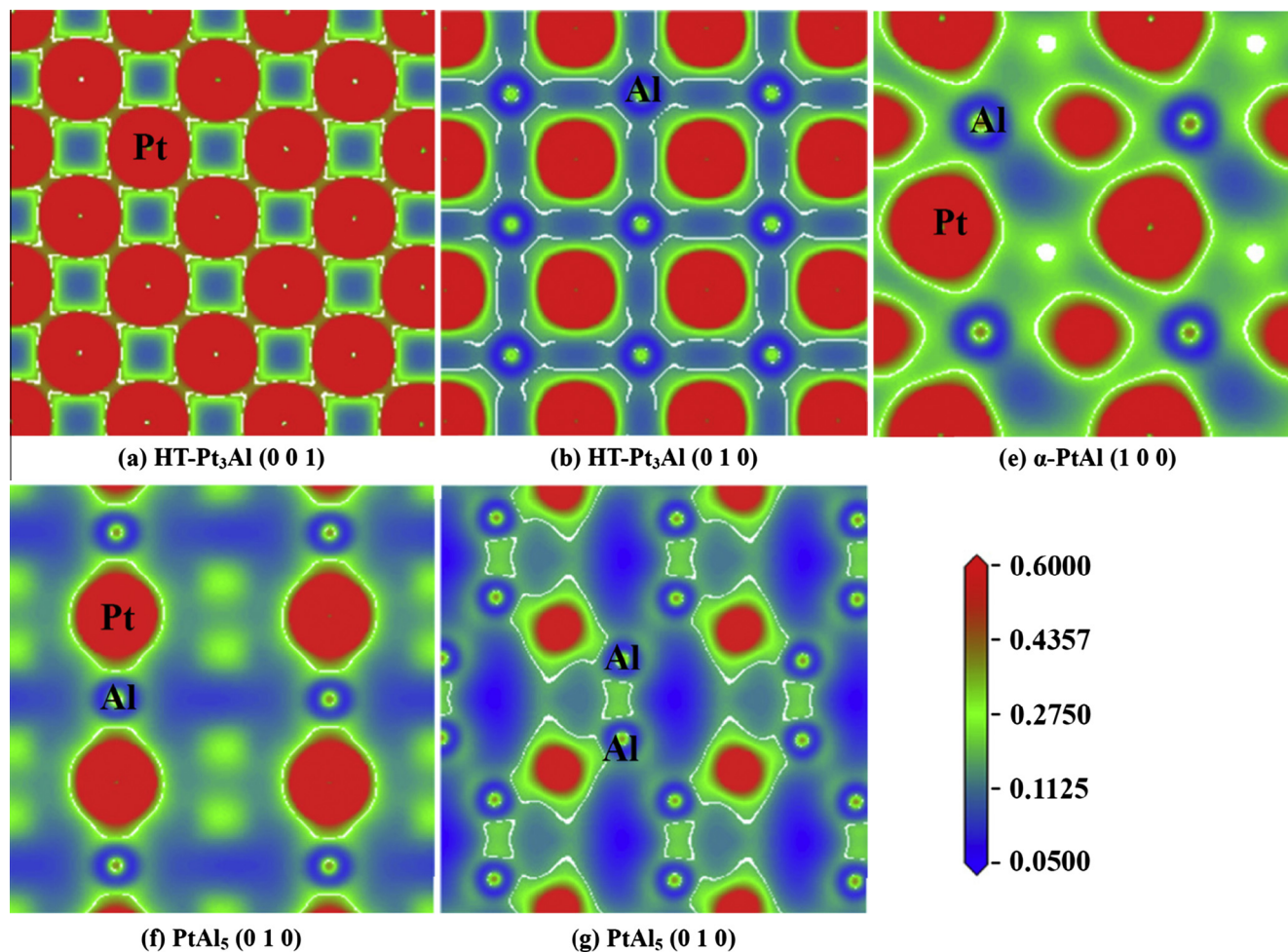


Fig. 6. Contour plot of charge density of HT-Pt₃Al(a), α -PtAl (b) and PtAl₅ (c);

HT-Pt₃Al. With the increasing Al concentration, the hybridization between Pt-5*d* and Al-3*p* orbitals decreases and the hybridization between Al-3*s* and Al-3*p* orbitals increases. Finally, the relatively strong Al–Al covalent interactions become dominant in PtAl₅ phase. The relatively strong covalent interaction of Al–Al in PtAl₅, and Pt–Al in HT-Pt₃Al should be responsible for their good structural stability and outstanding mechanical properties.

Acknowledgements

This work is supported by National Natural Science Foundation of China (NSFC) under Grants Nos. 51201148, U1530402 and 51071140. L. Wu thanks the foundation of Hebei Province Education Department under Grant No. QN2014114 and the Autonomic Research Project of Yanshan University under Grant No. 13LGB007.

Appendix A. Supplementary material

Supplementary data associated with this article can be found, in the online version, at <http://dx.doi.org/10.1016/j.commatsci.2016.08.003>.

References

- [1] R. Sot, K.J. Kurzydowski, Ab initio calculations of elastic properties of Ni₃Al and TiAl under pressure, *Mater. Sci.-Poland* 23 (2005) 587–590.
- [2] D. Shi, B. Wen, M. Roderick, S. Yao, T.-J. Li, First-principles studies of Al–Ni intermetallic compounds, *J. Solid State Chem.* 182 (2009) 2664–2669.
- [3] D.E. Kim, S.L. Shang, Z.K. Liu, Effects of alloying elements on elastic properties of Ni₃Al by first-principles calculations, *Intermetallics* 18 (2010) 1163–1171.
- [4] B. Wen, J.-J. Zhao, F.-D. Bai, T.-J. Li, First-principle studies of Al–Ru intermetallic compounds, *Intermetallics* 16 (2008) 333–339.
- [5] M.B. Cortie, A. Maarof, G.B. Smith, P. Ngoepe, Nanoscale coatings of AuAl_x and PtAl_x and their mesoporous elemental derivatives, *Curr. Appl. Phys.* 6 (2006) 440–443.
- [6] S. Cui, D.Q. Wei, Q. Zhang, Q. Zhang, Z. Gong, H. Hu, Newly found phase transition and mechanical stability of AuAl₂: a first-principles study, *J. Alloys Comp.* 574 (2013) 486–489.
- [7] H.Y. Wu, Y.H. Chen, C.R. Deng, X.F. Su, Elastic and thermodynamic properties of AuAl₂ under pressures, *J. Alloys Comp.* 528 (2012) 115–2210.
- [8] H.R. Chauke, B. Minisini, R. Drautz, D. Nguyen-Manh, P.E. Ngoepe, D.G. Pettifor, Theoretical investigation of the Pt₃Al ground state, *Intermetallics* 18 (2010) 417–421.
- [9] L.A. Cornish, R. Süß, A. Douglas, L.H. Chown, L. Glaner, The Platinum Development Initiative: Platinum-based alloys for high temperature and special applications: Part I, *Platinum Met. Rev.* 53 (2009) 2–10.
- [10] P.J. Hill, N. Adams, T. Biggs, P. Ellis, J. Hohls, S.S. Taylor, I.M. Wolff, Platinum alloys based on Pt–Pt₃Al for ultra-high temperature use, *Mater. Sci. Eng., A* 329 (2002) 295–304.
- [11] A. Douglas, J.H. Neethling, R. Santamarta, D. Schryvers, L. Cornish, Unexpected ordering behaviour of Pt₃Al intermetallic precipitates, *J. Alloys Comp.* 432 (2007) 96–102.
- [12] V. Raghavan, Al–Pt–Ti (Aluminum–Platinum–Titanium), *J. Phase. Equilib. Diff.* 33 (2012) 147–148.
- [13] D.P. Adams, M.A. Rodriguez, P.G. Kotula, Rhombohedral AlPt Films Formed by Self-Propagating, High Temperature Synthesis, Sandia National Laboratories, 2005.
- [14] C. Weidenthaler, W. Brijoux, T. Ould-Ely, B. Spliethoff, H. Bönemann, Synthesis and characterization of a new modification of PtAl, *Appl. Organomet. Chem.* 17 (2003) 701–705.
- [15] J.H. Sun, H.C. Jang, E. Chang, Effects of pretreatments on structure and oxidation behaviour of dc-sputtered platinum aluminide coatings, *Surf. Coat. Technol.* 64 (1994) 195–203.

- [16] A.J. McAlister, D.J. Kahan, The Al–Pt (Aluminum–Platinum) system, *J. Phase Equilib.* 7 (1986) 47–51.
- [17] K. Chattopadhyay, P. Ramachandrarao, Metastable phase formation and decomposition in a rapidly solidified aluminium–platinum alloy, *Mater. Sci. Eng.* 38 (1979) 7–17.
- [18] K. Schubert, On the binding in phases of mixtures T^*B_3 , *Z. Kristallogr.* 148 (1978) 193–206.
- [19] M. Wörle, F. Krumeich, T. Chatterji, S. Kek, R. Nesper, On the structure and twinning of $PtAl_4$, *J. Alloys Comp.* 455 (2008) 130–136.
- [20] A.M. Tonejc, A. Bonefačić, Non-equilibrium phases in Al-rich Al–Pt alloys, *J. Mater. Sci.* 9 (1974) 523–526.
- [21] D.E. Kim, V.R. Manga, S.N. Prins, Z.-K. Liu, First-principles calculations and thermodynamic modeling of the Al–Pt binary system, *Calphad* 35 (2011) 20–29.
- [22] J. Feng, B. Xiao, J. Chen, Y. Du, J. Yu, R. Zhou, Stability, thermal and mechanical properties of Pt_xAl_y compounds, *Mater. Des.* 32 (2011) 3231–3239.
- [23] D. Vanderbilt, Soft self-consistent pseudopotentials in a generalized eigenvalue formalism, *Phys. Rev. B* 41 (1990) 7892.
- [24] J.A. White, D.M. Bird, Implementation of gradient-corrected exchange-correlation potentials in Car-Parrinello total-energy calculations, *Phys. Rev. B* 50 (1994) 4954.
- [25] J.P. Perdew, K. Burke, M. Ernzerhof, Generalized gradient approximation made simple, *Phys. Rev. Lett.* 77 (1996) 3865.
- [26] H.J. Monkhorst, J.D. Pack, Special points for Brillouin-zone integrations, *Phys. Rev. B* 13 (1976) 5188.
- [27] R. Hill, The elastic behaviour of a crystalline aggregate, *Proc. Phys. Soc. A* 65 (1952) 349.
- [28] Z.-J. Wu, E.-J. Zhao, H.-P. Xiang, X.-F. Hao, X.-J. Liu, J. Meng, Crystal structures and elastic properties of superhard IrN_2 and IrN_3 from first principles, *Phys. Rev. B* 76 (2007) 054115.
- [29] K. Wu, Z. Jin, Thermodynamic assessment of the Al–Pt binary system, *J. Phase Equilib.* 21 (2000) 221–226.
- [30] M. Born, K. Huang, *Dynamical Theories of Crystal Lattices*, Clarendon, Oxford, 1956.
- [31] S.K.R. Patil, B.R. Tuttle, J.K. Bording, S. Kodambaka, Mechanical stability of possible structures of PtN investigated using first-principles calculations, *Phys. Rev. B* 73 (2006) 104118.
- [32] R.E. Watson, M. Weinert, Transition-metal aluminide formation: Ti, V, Fe, and Ni aluminides, *Phys. Rev. B* 58 (1998) 5981.
- [33] S.F. Pough, Relations between the elastic moduli and the plastic properties of polycrystalline pure metals, *Philos. Mag.* 45 (1954) 823–843.
- [34] W.-C. Hu, D.-J. Li, X.-Q. Zeng, C.-S. Xu, First-principles study of structural and electronic properties of C14-type Laves phase Al_2Zr and Al_2Hf , *Comput. Mater. Sci.* 83 (2014) 27–34.
- [35] H. De Waal, R. Pretorius, Lateral diffusion study of the Pt–Al system using the NAC nuclear microprobe, *Nucl. Instrum. Methods Phys. Res., Sect. B* 158 (1999) 717–721.
- [36] W. Bronger, P. Müller, Zur Struktur platinreicher Aluminium–Platin-Legierungen, *Z. Anorg. Allg. Chem.* 623 (1997) 362–368.
- [37] T. Chattopadhyay, K. Schubert, Crystal structure of $Pt_3Ga(r)$ and of some phases of the alloy Pt–Al, *J. Less-Common Met.* 41 (1975) 19–32.
- [38] R. Huch, W. Klemm, Das system platin–aluminium, *Z. Anorg. Allg. Chem.* 329 (1964) 123–135.
- [39] M. Ellner, U. Kattner, B. Predel, Konstitutionelle und strukturelle untersuchungen im aluminiumreichen teil dersysteme Ni–Al und Pt–Al, *J. Less Common Met.* 87 (1982) 305–325.
- [40] Y.-G. Zhang, Y.-F. Han, G.-L. Chen, J.-T. Guo, *Intermetallics Structure Materials*, Science Press, Beijing, 2001.
- [41] G. Grimvall, *Thermophysical Properties of Materials*, Elsevier, North-Holland, Amsterdam, 1999.